HIGH-SPEED GENERAL PURPOSE DEMODULATION PIXELS BASED ON BURIED PHOTODIODES

Lysandre-Edouard Bonjour [1,2], Thomas Baechler[1], Maher Kayal [2]

[1] CSEM SA, Photonics Division, Technoparkstrasse 1, CH-8005 Zurich, Switzerland
[2] EPFL STI IEL GR-KA, Federal Inst. of Technology, CH-1015 Lausanne, Switzerland

phone: +41 44 497 14 57 **fax:** +41 44 497 14 00 **e-mail:** lysandre-edouard.bonjour@csem.ch

Abstract

Using a standard 0.18um CMOS process with a buried photodiode (BPD) option, test pixels with a single transfer gate were characterized. The test pixels enabled finding an optimized BPD layout that minimizes the potential barriers hindering the charge transfer. Demodulation pixels having a 6.3um pitch or less were then developed and demonstrated to demodulate light signals up to at least 50MHz. Moreover, charge transfer noise was highly reduced by optimizing the pixel operating conditions. Demodulation of single photoelectrons could thus be made possible.

1. Introduction

Both fluorescence lifetime imaging microscopy (FLIM) and 3D time-of-flight (3D-TOF) vision may be performed by solid-state image sensors using frequency or time domain demodulation principles.

In the so-called frequency domain, a periodic stimulus is used to illuminate a scene. The information (e.g. the fluorescence lifetime) is then extracted from the phase shift of the returning signal[1][2]. In the time domain, the information is extracted from the delay of a returning delta pulse of light. Time-correlated single-photon counting (TCSPC) using single photon avalanche diodes (SPADs) array and time-gated systems like intensified CCDs (ICCD) are best examples of the second category. On the one hand however, SPADs suffer from a limited integration capability, low fill factor and indirect signal gating during the dead time. Time-gated ICCDs on the other hand are expensive, bulky and part of the detectable signal is rejected due to signal gating. This paper presents a novel imaging method suitable for FLIM and the necessary pixel for time domain demodulation with increased detection capability.

2. Pixel architecture

The proposed demodulation pixel is shown in figure 1 with one possible layout implementation in figure 2. Its photosensitive element is implemented as a buried photodiode (BPD) with three transfer gates driven by the signals TX1, TX2 and TXR. They connect respectively to two different sense nodes and to a reference supply voltage to enable global photodiode reset. Also, while TXR may not be required for frequency domain demodulation, in the time domain it contributes to the

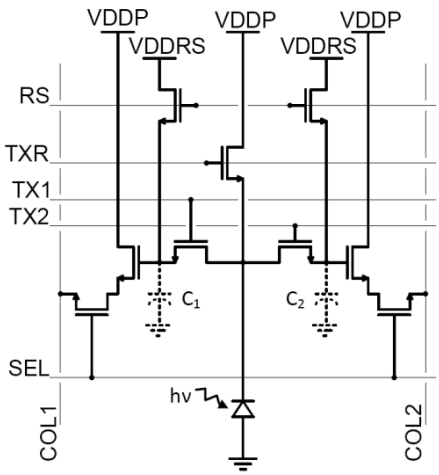

Fig. 1: Pixel architecture

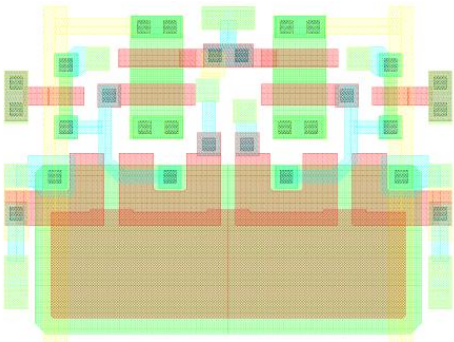

Fig. 2: BPD layout example

background suppression in 3D-TOF vision[3] and rejection of the excitation light in FLIM. Its function is presented in the timing diagram of figure 3. While the sample is illuminated by the burst of light, TXR is enabled, thus draining the reflected excitation light and the auto-fluorescence of the sample. TX1 and TX2 are then sequentially enabled to transfer the signal charges from the BPD to two different sense nodes. Assuming a mono-exponential decay and a negligible background light level, the lifetime τ may be extracted as:

$$\tau = \frac{t_A}{\ln\left(\frac{Q_A}{Q_B}+1\right)} \quad (1)$$

where t_A is the length of the TX1 pulse, allowing the collection of a charge Q_A on one sense node. The TX2

pulse of length t_B is then chosen long enough to collect the remaining signal charge Q_B in the second sense node. This rapid lifetime determination (RLD) method is a particular case of [4] with $t_A \neq t_B$ and $t_B \gg \tau$.

In practice, reflection from the excitation light burst on the sensor may lead to charge leakage on the two sense nodes, although the global photodiode reset is enabled. This offset may be removed by handling charges differentially. In that case, two frames are required for the lifetime estimation, leading to an equation analytically unsolvable for τ:

$$\frac{Q_{B_1}-Q_{A_1}}{Q_{B_2}-Q_{A_2}} = \frac{e^{-\frac{t_{A_1}+t_{B_1}}{\tau}}-2e^{-\frac{t_{A_1}}{\tau}}+1}{e^{-\frac{t_{A_2}+t_{B_2}}{\tau}}-2e^{-\frac{t_{A_2}}{\tau}}+1} \quad (2)$$

Equation 2 has a particular solution for τ if $t_{A_1} = t_{B_1}$, $t_{A_2} = t_{B_2}$ and $2t_{A_1} = t_{A_2}$, which in addition allows discarding the constant background light level:

$$\tau = -\frac{t_{A_1}}{\ln\left(\sqrt{\frac{Q_{B_2}-Q_{A_2}}{Q_{B_1}-Q_{A_1}}}-1\right)} \quad (3)$$

In this RLD method, t_{A_1} may be chosen in such a way that virtually no signal charge is gated away ($2t_{A_1} \gg \tau$), thus taking advantage of the entire detectable signal impinging on the sensor.

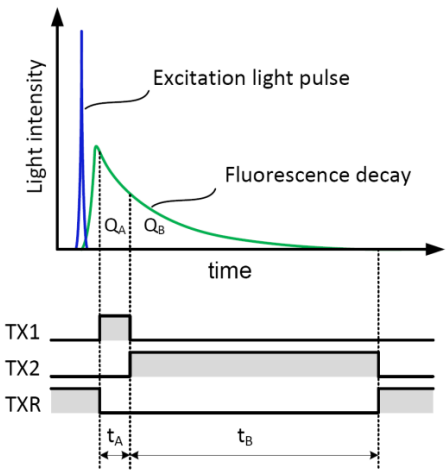

Fig. 3: Proposed timing diagram for fluorescence lifetime estimation in FLIM applications. The excitation pulse can be discarded by activating TXR.

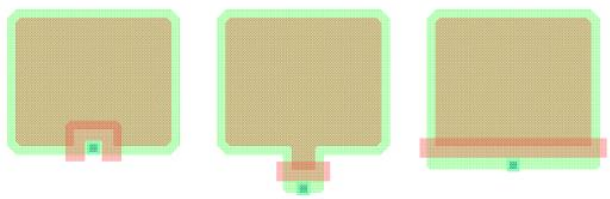

Fig. 4: BPD layouts characterized for charge transfer speed. From left to right, diode G1, G6 and G7.

3. Buried photodiode optimization

3D-TOF vision in an operating range of a few meters and FLIM applications requiring lifetime measurements of a few nanoseconds need demodulation pixels working at frequencies of several tens of megahertz. A short transfer time of photoelectrons from the BPD to the sense node is therefore critical for these applications. The BPD shape and size as well as the transfer gate shape are key elements to be optimized to provide an electrostatic potential distribution in the BPD favorable to the charge transfer[5]. However, exotic BPD shapes proposed for pixel pitches larger than 10um[6][7] become less suitable when increasing the resolution of image sensors because of the already limited fill factor. Alternatively, optimization of the transfer gate shape may be performed.

BPDs of about 5.4um x 4.4um with variations in transfer gate shape (figure 4) were produced in test fields of 16x16 pixels. They were characterized for charge transfer speed with the gate operated at 3.0V and a sense node reset voltage of 2.5V. The illumination has been set so that after complete charge transfer the measured signal level corresponds to about 10% of the sense node full well. The normalized output signal as a function of the transfer time is presented on figure 5.

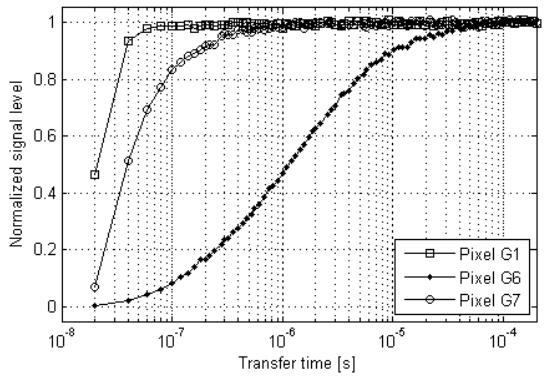

Fig. 5: Normalized signal level measured on the sense node as a function of the charge transfer time. The measured signal level corresponds to about 10% of the sense node full wells.

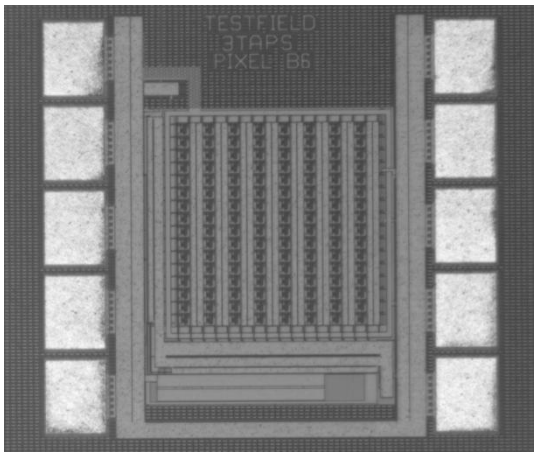

Fig. 6: One test field with 16x8 pixels.

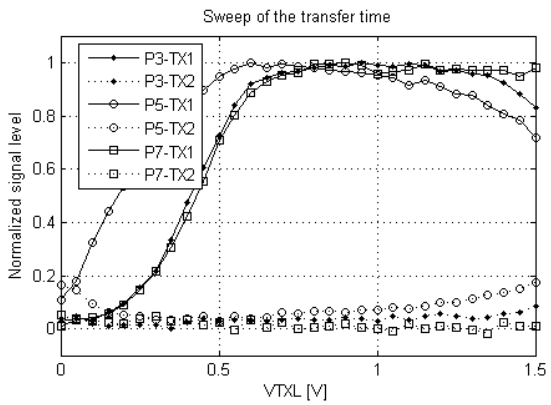

Fig. 7: Output signals after 1000 demodulations cycles on three different BPDs (P3, P5, P7) as a function of the TX-signals lower reference voltage. TX1 is always activated prior to TX2.

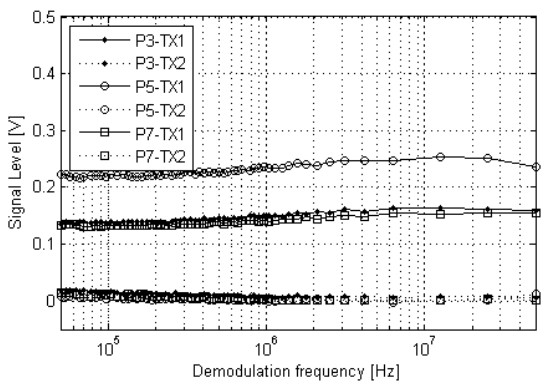

Fig. 8: Output signals of three different pixels as a function of the demodulation frequency. The measurement is performed after 1000 demodulation cycles prior to readout. TX1 is always activated prior to TX2.

Pixel G1, with a U-shaped transfer gate, has the best characteristic with complete transfer in less than 80ns. Conversely, G6 suffers from a large potential barrier due to the pinching region in front of the transfer gate leading to complete transfer in about 100us. Gates protruding into the BPD are therefore the most efficient in reducing the electrostatic potential barrier and thus improving the transfer speed. They are therefore best suited for demodulation pixels.

4. Measurements on demodulation pixels

Eight different BPDs were designed as proposed in the pixel architecture of figure 1 and characterized in test fields of 16x8 pixels as shown in figure 6. The pixel layouts fit a 6.3um pitch and have a drawn fill factor of 12.5% to 32%. The demodulation functionality is verified through contrast measurements with a 670nm VCSEL used as pulsed light source. After a 10ns light pulse, a hold-time of 330ns is observed to let photoelectrons generated deep in the substrate diffuse up to the BPD. TX1 and TX2 are then toggled, followed by a TXR pulse of 120ns to drain any remaining photoelectrons. The hold time introduced after the excitation pulse in this measurement is not considered to be limiting because in FLIM it is not expected to be necessary when measuring lifetimes at shorter wavelengths. On the contrary, 3D-TOF requires excitation wavelengths in the near-infrared. In this particular application, the silicon substrate may require some modifications to allow real time demodulation.

It was noticed under low light conditions, where statistically less than one photoelectron is generated in the BPD per demodulation cycle, that charge transfer noise may dominate. Under standard operating conditions, the measured contrast becomes close to zero after 1000 demodulation cycles at such a low illumination levels. On the contrary, at 50Mhz the contrast becomes higher than 90% with excellent symmetry when optimizing the shape of the TX-signals. The off-chip TX drivers were modified to prevent undershoots and to allow the lower reference voltage V_{TXL} to be increased above 0V. Figure 7 depicts the normalized signal level on both sense nodes as a function of V_{TXL} for three different BPDs (P3, P5 and P7). The measurement is performed after 1000 demodulation cycles with statistically 1.5 to 3 photoelectrons generated in the BPDs per light burst, corresponding to about 10 to 20% of the sense node full well after charge transfer. Demodulation becomes effective already at V_{TXL}=0.6V for P5 whereas a higher level of 0.8V is necessary for P3 and P7. This difference can be attributed to the higher fill factor of P5. Indeed in P5, the charge packet handled in each demodulation cycle is larger, hence the charge transfer noise has a lower impact in this measurement. The charge transfer noise, attributed to charge trapping and de-trapping at the Si-SiO_2 interface is thus largely reduced by increasing V_{TXL}.

With V_{TXL}=0.8V, contrast measurements are plotted against the demodulation frequency on figure 8 and figure 9. Note that the demodulation frequency is defined as one over the total time of the TX1 and TX2 pulses in a demodulation cycle. Figure 8 shows the output signal on each sense node as a function of the demodulation frequency, while first transferring through the gate driven by TX1. Figure 9 depicts the normalized contrast for each pixel while the first transfer is either performed through the gate driven by TX1 or by the one driven by TX2. This graph provides a method to verify the symmetry of the different pixels. Although all of them show a very good symmetry over frequencies, a contrast loss at 50Mhz is observed for pixels P3 and P5. However, pixel P7 stays fast enough until at least 50Mhz, the frequency limit being out of reach of the used characterization setup.

Finally, figure 10 shows an illumination sweep with the already described operating conditions. Pixel P5 again has a different characteristic due to its higher fill factor. All three pixels show a good demodulation capability and linearity at low-light levels.

5. Future work

A sensor with a resolution of 256x256 demodulation pixels of the type presented on figure 1 was designed and is currently under characterization. The driving circuitry was adapted to allow rolling shutter readout and automatic modification of the TX1 and TX2 pulse lengths between odd and even frames. This will allow the implementation of the RLD method proposed in equation 3. Functional as well as application specific characterization for FLIM and 3D-TOF will be performed.

6. Conclusion

Demodulation pixels of 6.3um pitch based on BPDs were designed and characterized. A contrast of over 90% was demonstrated after 1000 demodulation cycles at 50MHz thanks to optimized pixel layouts. Charge transfer noise was shown to have a large impact on the demodulation efficiency and was largely reduced by optimizing the shape of the signals driving the transfer gates.

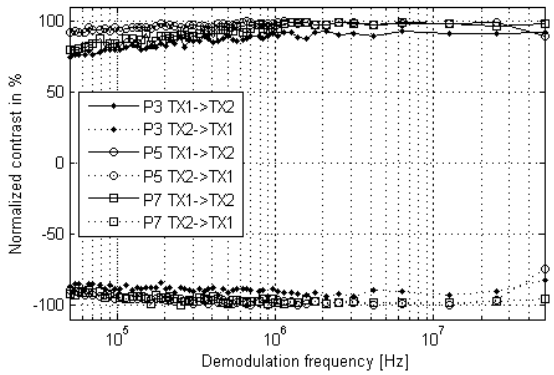

Fig. 9: Normalized contrast measured on three different pixels. The measurement is performed after 1000 demodulation cycles. Toggling in both TX1→TX2 and TX2→TX1 order is depicted.

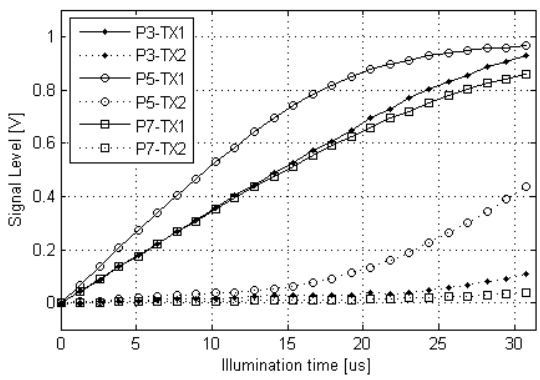

Fig. 10: Output signals of three different pixels as a function of the illumination time. The measurement is performed with 1000 demodulation cycles at 50MHz. TX1 is activated prior to TX2.

[1] B. Büttgen, T. Oggier, R. Kaufmann, P. Seitz and N. Blanc, « Demonstration of a novel drift field pixel structure for the demodulation of modulated light waves with application in three-dimensional image capture », Proc. of SPIE-IS&T electronic imaging, vol. 5302, 2004

[2] A. Esposito, T. Oggier, H.C. Gerritsen, F. Lustenberger and F.S. Wouters, « All-solid-state lock-in imaging for wide-field fluorescence lifetime sensing », Optics express, vol. 13, no. 24, 2005

[3] T. Sawada, K. Ita, M. Nakayama and S. Kawahito, « TOF range image sensor using a range-shift technique », IEEE Sensors conference, 2008

[4] R.M. Ballew and J.N. Demas, « An error analysis of the rapid lifetime determination method for the evaluation of single exponential decays », Anal. chem., vol. 61, p.30-33, 1989

[5] H. Mutoh, « 3-D optical and electrical simulation for CMOS image sensors », International Image Sensor Workshop, 2003

[6] C. Tubert, L. Simony, F. Roy, A. Tournier, L. Pinzelli, P. Magnan, « High speed dual port pinned-photodiode for time-of-flight imaging », International Image Sensor Workshop, 2009

[7] H. Takeshita, T. Sawada, T. Iida, K. Yasutomi and S. Kawahito, « High-speed charge transfer pinned-photodiode for CMOS time-of-flight range image sensor », Proc. of SPIE-IS&T electronic imaging, vol. 7536, 2010